

www.acsami.org Research Article

# Leveraging the Assembly of a Rylene Dye to Tune the Semiconducting Properties of Functionalized n-Type, Hybrid Si Interfaces

Arindam Mukhopadhyay, Victor Paulino, Kaixuan Liu, Carrie L. Donley, Brianna Bernard, Alfred Shomar, Chuan Liu, and Jean-Hubert Olivier\*



Cite This: ACS Appl. Mater. Interfaces 2021, 13, 4665-4675



**ACCESS** 

Metrics & More

Article Recommendations

s Supporting Information

**ABSTRACT:** The functionalization of silicon electrodes with  $\pi$ -conjugated chromophores opens new avenues to engineer hybrid semiconducting interfaces relevant to information storage and processing. Notably, molecularly dissolved  $\pi$ -conjugated units, such as ferrocene derivatives, are traditionally exploited as building blocks to construct well-defined interfaces that establish electrochemically addressable platforms with which to investigate electron transfer properties and charge storage capabilities. In contrast, planar  $\pi$ -conjugated building blocks such as naphthalene diimide (NDI) cores enable the formation of solvated aggregates equipped with emergent electronic structures not manifested by the parent, molecularly dissolved building blocks. To interrogate the extent to which the aggregated states of  $\pi$ -conjugated chromophores can be leveraged to regulate the n-type semiconducting properties of

functionalized electrodes, we have devised an amphiphilic rylene core (NDI) that demonstrates a non-negligible degree of aggregation in an aqueous medium. Characterization of the electronic structures of the NDI-derived aggregates using a combination of electrochemistry, reductive titration experiments, and spectroelectrochemistry unveils the existence of  $\pi$ -anion stacks, the formation of which is contingent on the initial concentration of NDI building blocks. We show that grafting n-doped NDI aggregates on silicon electrode precursors equipped with a high density of anchoring groups by means of "click" reaction enables the formation of the hybrid Si-NDI electrode (Si-NDI-15@1) that facilitates electron injection by more than 400 mV when compared to Si interfaces constructed from molecularly dissolved NDI units. Furthermore, the engineering of a Si precursor surface characterized by a low density of anchoring groups provides additional proof to highlight that the potentiometric properties recorded for Si-NDI-15@1 originate from NDI units, evidencing a non-negligible degree of aggregation. The present work delivers tools to manipulate the potentiometric properties of functionalized electrodes by leveraging on the electronic structures of aggregated,  $\pi$ -conjugated precursors.

KEYWORDS: silicon electrode functionalization, naphthalene diimide, semiconducting nanostructures, n-doped aggregate, semiconducting interfaces

## **■** INTRODUCTION

The development of functional materials paves the way to fabricate smart integrated devices for applications in optoelectronics, information storage technology, and energy transduction schemes.  $^{1-5}$  In particular, the enticing optical and electronic properties of organic nanomaterials built from  $\pi$ -conjugated building blocks have bolstered this class of materials as promising candidates to engineer organic field-effect transistors,  $^{6,7}$  spin valves and filters,  $^{8-11}$  organic solar cells,  $^{12-15}$  and chemical sensors.  $^{16,17}$  The interfaces defined by the organic semiconducting media and the inorganic electrodes play a cardinal role in dictating the efficiency of these devices.  $^{18-21}$  Consequently, the last few decades have witnessed a surge in interest to develop strategies to

functionalize (semi)conducting surfaces with redox-active molecular systems using a bottom-up approach.<sup>22–24</sup> The resulting hybrid electrodes have provided unique platforms to not only unveil the parameters that regulate interfacial electron-transfer processes and electron-spin filtering effects but also elucidate electrocatalytic cycles.<sup>14,25,26</sup>

Received: October 13, 2020 Accepted: December 22, 2020 Published: January 14, 2021





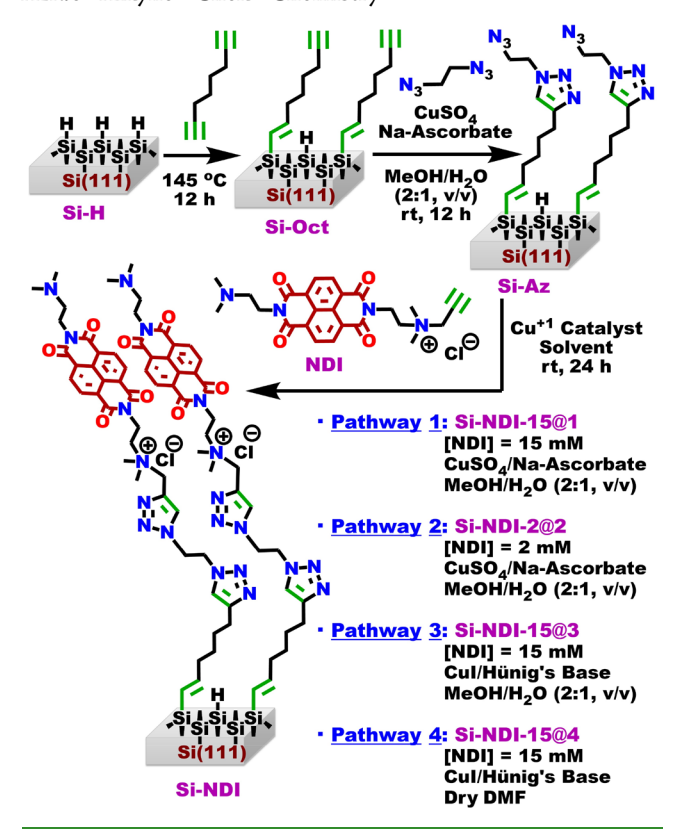
The covalent functionalization of doped silicon (Si) surfaces with redox-active organic constructs enables the formation of chemically well-defined, thermally robust, and electronically responsive nanoarchitectures at Si/organic interfaces. Strategies to covalently functionalize hydrogen-terminated monocrystalline silicon (oxide-free) surfaces (Si-H) with a broad variety of redox-active chromophores have gained considerable attention and represent a compelling approach to engineer integrated systems for functional electronic devices. 24,27-36 More specifically, seminal studies have unambiguously demonstrated that synthetic grafting strategies can be modulated to control the density of redox-active constructs on Si-H surfaces, delivering hybrid surfaces equipped with tailored electrochemical properties. <sup>24,27-41</sup> For example, the spatial proximity of anchored redox units engenders local electronic interactions that regulate the potentiometric properties of the semiconducting hybrids. 22-24 Pioneering studies have reported the anchorage of ferrocene redox reporters on silicon surfaces with a surface density as high as  $3.5 \times 10^{-10}$ mol cm<sup>-2</sup>, indicating the formation of a packed monolayer where non-negligible electronic interactions between the ferrocene heads have been confirmed by scanning electrochemical microscopy investigations.<sup>39</sup> The high surface coverage reported for Si substrates is the combined product of a surface confinement effect along with robust Si-C bonds that provide monolayer-thick materials equipped with electronic functions which differ from those of the building blocks in solution.

While the construction of hybrid silicon interfaces that feature electron donor (p-type) monolayers is well established, 22-24,27,28,31,36,37,40,42 only a handful of studies have only a handful of studies have reported the anchoring of electron acceptor (n-type) building blocks. The low reduction potential of the redox-active naphthalene diimide (NDI) cores, which are a class of rylene dyes, renders this class of chromophores an appealing candidate to devise n-type semiconducting interfaces that feature a low-lying conduction band energy. 43-51 We have recently reported that a synthetic approach involving thermal grafting of an aliphatic alkadiyne on a p-doped Si-H surface followed by Cu1+-catalyzed "click" reaction enables the formation of reactive monolayers on which NDI cores are grafted. S2 Contrasting the reversible redox properties measured for the solvated NDI precursors, the NDI-functionalized Si interfaces (Si-NDIs) exhibit quasi-irreversible electrochemical behavior that may suggest structural perturbation of the anchored monolayer upon n-doping in addition to slow electron transfer processes. Moreover, the  $\pi-\pi$  interactions between anchored neighboring NDI cores may lead to the formation of a collection of electronic states that are energetically disparate. Furthermore, while the NDI building blocks are present as molecularly dissolved in solution, the high density of reactive functional groups featured on the precursor Si-H surface can enable the confinement of the NDI cores, consequently enforcing electronic coupling between redoxactive units. The extent to which the aggregation properties of NDI cores in solution can be harnessed to modulate the potentiometric properties of Si-NDI interfaces remains elusive, yet it can deliver tools to modulate the semiconducting properties of hybrid materials.

Controlling the assembly of  $\pi$ -conjugated chromophores enables the formation of aggregates equipped with tunable structure—function relationships. 53-56 Dispersion forces and quadrupole-quadrupole interactions are parameters governing the aggregation of  $\pi$ -conjugated cores in solution. <sup>57–59</sup> The assembly properties of NDI chromophores have been wellestablished and provide access to solvated superstructures with optical and electronic properties that differ from those evidenced by molecular precursors. 60-62 In these assemblies, interchromophoric interactions enforce the formation of electronic states that trace their origin from modest to strong coupling of frontier molecular orbitals. 63-66 Combining the assembly properties of NDI aggregates with the electrical properties of the Si-H surface opens new avenues to not only regulate the electronic properties of hybrid semiconducting surfaces but also establish strategies to leverage the structurefunction properties of solvated,  $\pi$ -conjugated aggregates.

Herein, we establish that grafting the amphiphilic NDI chromophore shown in Scheme 1, initially under an aggregated

Scheme 1. Access to NDI-Functionalized Hybrid Si(111) Interfaces (Si-NDI) Based on Initial Thermal Grafting Followed by Sequential Postsynthetic Modifications Using Azide-Alkyne "Click" Chemistry



state or as molecularly dissolved, on a conducting silicon electrode provides a means to regulate the potentiometric properties of the final semiconducting interfaces Si-NDIs. Our method exploits an azide-terminated Si surface (Si-Az) that, by presenting a high density of reactive functional groups, allows the covalent confinement of the solvated NDI species via a Cu<sup>1+</sup>-catalyzed Huisgen 1,3-dipolar cycloaddition ("click" reaction). Exploiting the reaction pathways shown in Scheme 1, we show that the anchorage of NDI-derived aggregates on the Si surface enables the formation of semiconducting hybrid materials which facilitate electron injection by more than 400 mV when compared to interfaces exploiting molecularly dissolved NDI units as precursors (Pathway 1, Scheme 1). The noninnocent role played by the conformation of the NDI

chromophores at the interface is further supported from "surface dilution" experiments. This study confirms that the potentiometric properties of hybrid Si-NDI interfaces can be regulated by leveraging the initial aggregation states of the NDI-based redox probe, which, in turn, are controlled by varying the reaction conditions of the final covalent grafting step (Pathways 1–4, Scheme 1).

## ■ RESULTS AND DISCUSSION

The three-step synthetic approach leveraged to access the NDI-functionalized hybrid Si(111) interfaces (Si-NDIs) is chronicled in Scheme 1. Please refer to Section 2A in the Supoprting Information for details. Because the covalent functionalization of Si-H with aliphatic alkynes and alkadiynes is recognized to afford high surface coverage, 41,52 we exploited this principle to modify Si(111, p-type)-H surfaces by a thermally activated grafting process with 1,7-octadiyne (step 1) to construct the Si-Oct interfaces. Postsynthetic modification of the Si-Oct precursors with 1,2-diazidoethane via a "click" reaction provides the formation of the Si-Az platforms on which to further anchor the asymmetric NDI core that features an ammonium side chain terminated by an alkyne function.<sup>5</sup> Because the asymmetric NDI core is equipped with only one reactive side chain, the uncontrolled growth of multilayers on the Si-Az precursors is an unlikely process.

To modulate the aggregation state of the NDI cores involved in the construction of the final hybrid semiconducting interfaces Si-NDIs, Pathways 1 and 2 shown in Scheme 1 were explored first. Because the concentration of building blocks is a cardinal parameter governing the formation of noncovalent assemblies, we started by interrogating the aggregation state of NDI cores at high concentration (Pathway 1, [NDI] = 15 mM,  $[NDI]^{15 \text{ mM}}$ ) and low concentration (Pathway 2, [NDI] = 2mM, [NDI]<sup>2 mM</sup>). Please note that these conditions are to be exploited for the "click" reaction in Step 3 (Scheme 1). Because the electronic absorption properties of  $\pi$ -conjugated chromophores are highly sensitive to aggregation, we used ground-state electronic absorption spectroscopy to glean further information on the aggregated state of the NDI building block shown in Scheme 1. Figure 1A highlights the spectroscopic signatures of individualized NDI units that are unambiguously detected at [NDI] = 2 mM. The resolved 0-0, 0-1, and 0-2 vibronic transitions centered at 380, 359, and 341 nm, respectively, are consistently separated by 180 meV (1452 cm<sup>-1</sup>, C=C stretching), which is a hallmark of molecularly dissolved rylene diimide species. The addition of up to 1 equiv of the reductant, sodium ascorbate (NaAsc), used in the "click" reaction" does not alter the spectroscopic properties of the NDI building blocks as attested by the lack of emergent spectroscopic signatures.

In sharp contrast, the absorptive features characterizing the 15 mM NDI solution differ dramatically from those recorded for the individualized NDI species. In the absence of NaAsc, the ratio of the intensity of the 0–0 and 0–1 vibronic transitions centered at 381 and 360 nm, respectively, is below one, a spectroscopic fingerprint of electronically coupled NDI units. Furthermore, the addition of up to 1 equiv of the sacrificial electron donor (NaAsc) is accompanied by the rise of a new absorptive feature centered at 446 nm and the apparition of a broad absorption band in the NIR spectral window. Please note that these spectroscopic signatures are exclusively monitored during the reductive titration of a high concentration of NDI building blocks (Pathway 1, Scheme 1;

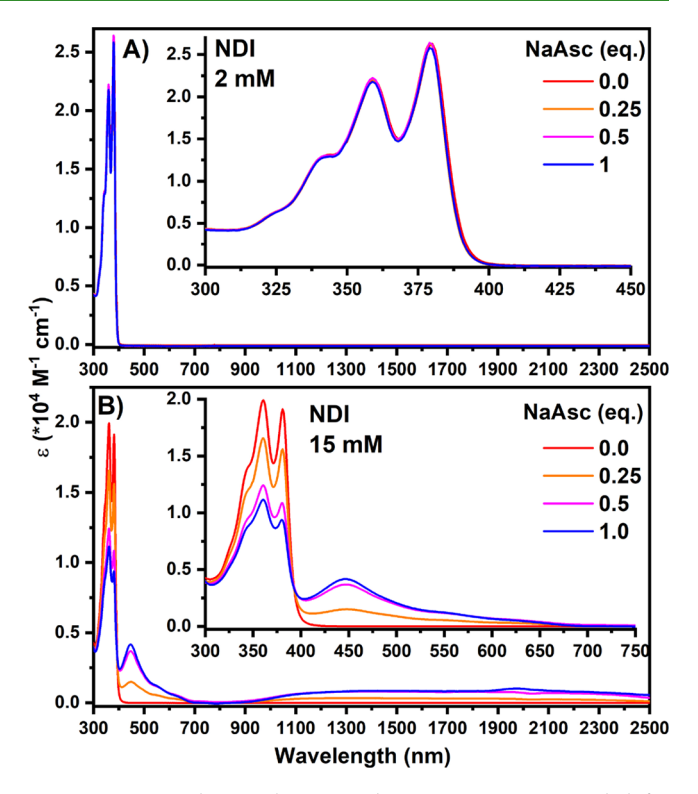


**Figure 1.** Ground-state electronic absorption spectra recorded for NDI building blocks in a mixture of  $CD_3OD/D_2O$  (2:1, v/v) as a function of the initial building block concentration (A = 2 mM, B = 15 mM) and upon addition of the sacrificial electron donor sodium ascorbate (NaAsc) at 25 °C. Optical path length = 0.1 mm.

[NDI] = 15 mM). This observation underscores the emergence of electronic states only accessed in the "click" reaction pathway, exploiting 15 mM concentration and the sacrificial electron donor. The origin of the broad NIR transition that spans the 900–2500 nm window has been previously attributed to spectroscopic states stemming from charge transfer and electron–electron interaction of NDI radical anions. <sup>43,46,48,63,64,66</sup>

Probing the potentiometric properties of NDI units as a function of concentration further reveals disparities in the electronic structure of the redox-active building blocks in  $[{\rm NDI}]^{2~{\rm mM}}$  and  $[{\rm NDI}]^{15~{\rm mM}}$ . As gleaned in Figure 2, the cyclic voltammograms recorded for the low and high concentration of NDI units show a partially irreversible cathodic transition with associated cathodic  $(E^{({\rm pl})})$  and anodic peaks  $(E^{({\rm p3})})$  centered at  $-0.477~{\rm V}$  vs Ag/AgCl and  $-0.102~{\rm V}$  vs Ag/AgCl for  $[{\rm NDI}]^{2~{\rm mM}}$  and  $-0.333~{\rm V}$  vs Ag/AgCl and 0.063 V vs Ag/AgCl for  $[{\rm NDI}]^{15~{\rm mM}}$ . The partially irreversible behavior demonstrated by both  $[{\rm NDI}]^{2~{\rm mM}}$  and  $[{\rm NDI}]^{15~{\rm mM}}$  may be attributed to a slow electron transfer process in addition to structural reorganization of NDI units, enforced upon reduction. Redox-active NDI building blocks are notorious for initiating the formation of charge-transfer dimers and larger  $\pi$ -anion stacks.  $^{63}$ 

To glean more information on the electronic structures of the NDI units in  $[\mathbf{NDI}]^{2~\mathrm{mM}}$  and  $[\mathbf{NDI}]^{15~\mathrm{mM}}$ , we estimated the potential  $E^{(i)}$  at the inflection point of the cathodic waves. This approach has been reported by Vullev et al. to provide the best approximation of the half-wave potentials  $(E^{(1/2)})$  for non-reversible electrochemical systems. The  $E^{(i)}$  is extrapolated from the first derivatives of the cyclic voltammograms shown

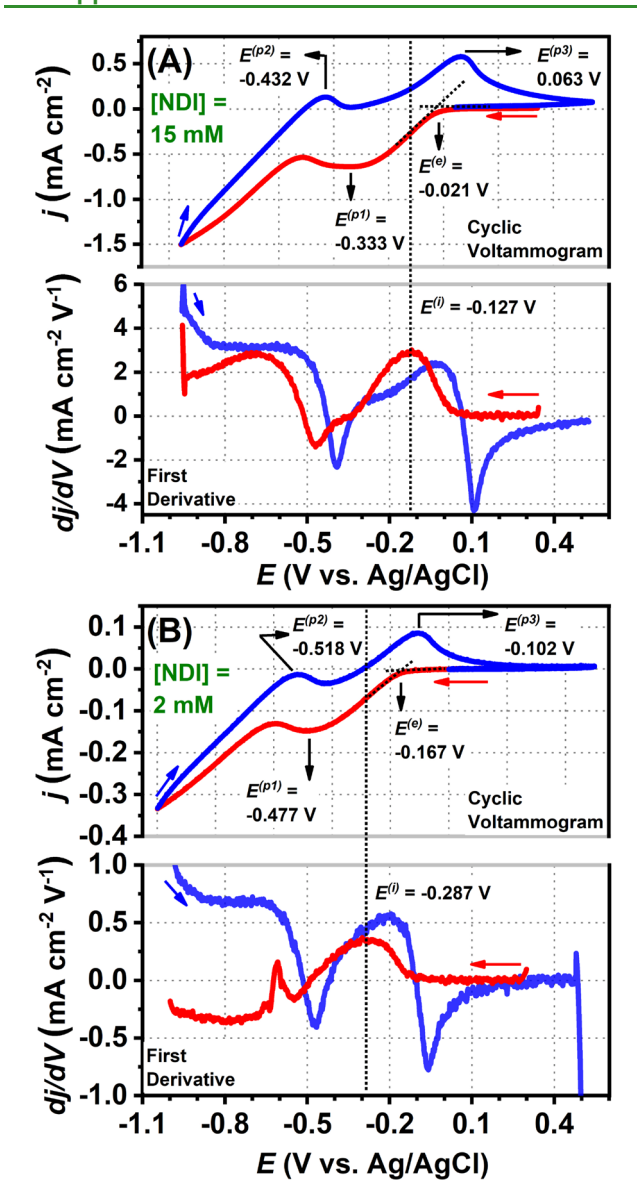


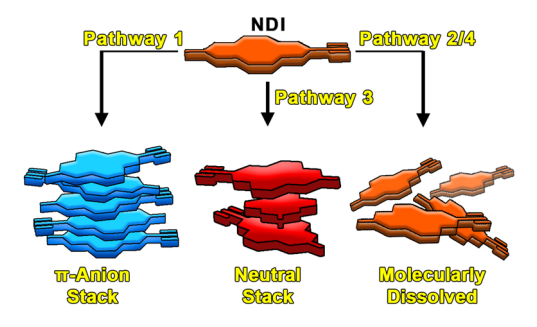
**Figure 2.** Cyclic voltammograms and their first derivative plots (scan rate =  $0.025 \text{ V s}^{-1}$ ) of the NDI building block at the concentration of 15 mM (A) and 2 mM (B) recorded in MeOH/H<sub>2</sub>O (2:1, v/v) using glassy carbon as the working electrode, Ag/AgCl (3 M NaCl) as the reference electrode, and Pt as the counter electrode under Ar gas atmosphere at 25 °C. We also wish to underscore the fact that the voltammograms were recorded in the absence of any externally added supporting electrolyte by keeping in mind that the molecular structure of the NDI building block already incorporates a terminal ammonium side chain.

in Figure 2A and 2B. In addition, edge potentials  $(E^{(e)})$  are reported. When compared to  $[\mathbf{NDI}]^{2~\mathrm{mM}}$ , the more anodic  $E^{(i)}$  elucidated for  $[\mathbf{NDI}]^{15~\mathrm{mM}}$  ( $\Delta E^{(i)} = 160~\mathrm{mV}$ ) suggests a nonnegligible stabilization of the reduction potentials of the NDI units as a function of the building block concentration. This observation corroborates the reductive titration experiments chronicled in Figure 1. The oxidation potential of NaAsc  $(E^{-/0} = 0.04~\mathrm{V}~\mathrm{vs}~\mathrm{Ag/AgCl})$  does not provide a sufficient driving force to reduce the NDI units in  $[\mathbf{NDI}]^{2~\mathrm{mM}}.^{68}$  In contrast, the fact that the first reduction potential is anodically shifted in  $[\mathbf{NDI}]^{15~\mathrm{mM}}$  indicates the existence of electronic states poised to oxidize the sacrificial electron donor NaAsc.

Spectroelectrochemistry experiments performed on the NDI building blocks corroborate the formation of  $\pi$ -anion stacks generated chemically during the addition of NaAsc. Please refer to Section 4 in the Supporting Information for details. As observed in Figure S4 which chronicles the electrochemically generated spectra, the excursion toward cathodic potentials (0.0 V to -0.7 V vs Ag/AgCl) is associated with drastic changes in the absorptive features characterizing the nascent species. A decrease of the absorption bands associated with the neutral NDI aggregate accompanies the rise of new transitions centered at 450, 535, 612, and 738 nm. In addition, the emergence of a broad NIR band that spans from 900 to 2500 nm observed in Figure S5 diagnoses the formation of  $\pi$ -anion stacks as reported by us and others. 63,66,69,70 Further excursion toward the cathodic potentials (-0.7 V to -1.0 V vs Ag/AgCl)initiates the apparition of spectroscopic features reminiscent to those of the NDI dianion species as chronicled in Figures S4 and S5.

The electronic absorptive properties and the electrochemical properties recorded for the NDI units in solution allow us to gain more insight into the aggregation state of the building blocks that are summarized in Scheme 2. While a low

Scheme 2. Illustration of the Aggregated State of the NDI Core As a Function of the Pathways Used to Functionalize the Si Precursor Si-Az<sup>a</sup>



 $^a$ Pathway 1: [NDI] = 15 mM; CuSO<sub>4</sub>/NaAsc; MeOH/H<sub>2</sub>O (2:1) v/v. Pathway 2: [NDI] = 2 mM, CuSO<sub>4</sub>/NaAsc; MeOH/H<sub>2</sub>O (2:1) v/v. Pathway 3: [NDI] = 15 mM; CuI/Hünig's Base; MeOH/H<sub>2</sub>O (2:1) v/v. Pathway 4: [NDI] = 15 mM; CuI/Hünig's Base; Dry DMF.

concentration of NDI building block (2 mM) in the MeOH/ H<sub>2</sub>O solvent mixture does not promote formation of an aggregated state (Pathway 2), increasing the concentration to 15 mM in MeOH/H<sub>2</sub>O solution (Pathway 3) is accompanied by a large degree of chromophore interaction and suggests that the chromophores exist primarily under the form of  $\pi$ -stacks. The electrochemical properties of  $[\text{NDI}]^{15~\text{mM}}$  in MeOH/H2O indicate the formation of electronic states that are stabilized when compared to those of the isolated building blocks. Consequently, the addition of a sacrificial electron donor (NaAsc) promotes the formation of  $\pi$ -anion stacks (Pathway 1, Scheme 2), exclusively formed at a high concentration of NDI (15 mM). Furthermore, even at high concentration (15 mM) in DMF solvent (Pathway 4, Scheme 2), the NDI cores manifest the hallmarks of a molecularly dissolved species as confirmed by the absorption spectrum shown in Figure S3.

Having established the structure—function relationships of NDI cores as a function of the designed pathways, the Si-Az surface precursors are functionalized, exploiting the "click" reactions following Pathways 1 and 2 in Scheme 1. The surface morphologies of the Si-NDI-15@1 and Si-NDI-2@2 inter-

faces were examined by tapping mode AFM and are shown in Figures 3A and S8, respectively. Interrogation of the root-

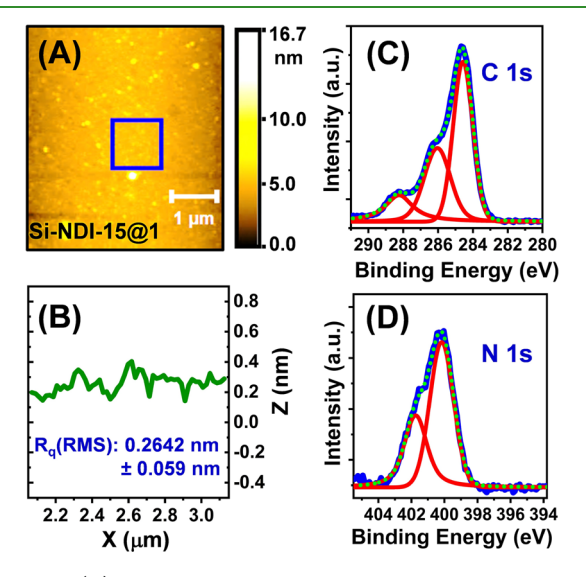


Figure 3. (A) Tapping mode AFM image of the Si-NDI-15@1 interface. (B) Cross-section profile of the area under the blue square on the AFM image depicted in (A) to determine the  $R_{\rm q}$  (RMS) roughness of the surface. (C and D) High-resolution XPS spectra (blue), deconvoluted spectra (red), and sum/fitted spectra (dotted green) of Si-NDI-15@1 that represent the C 1s (C) and N 1s (D) areas. Please note that the C 1s signal (C) can be deconvoluted into three Voigt functions with peaks centered at 288.2, 286.0, and 284.6 eV, which can be assigned to the contributions from C=O, C-N, and C-C bonds, respectively. On the other hand, the N 1s signal (D) can be deconvoluted into two Voigt functions with peaks centered at 401.9 and 400.1 eV that confirm the presence of chemically distinct nitrogen atoms.

mean-square (RMS) roughness ( $R_q$ ) parameter reveals that these two surfaces are smooth and atomically flat as attested by the  $R_{\rm q}$  (RMS) values below 0.5 nm. The chemical compositions of the hybrid Si-NDI interfaces were interrogated using high-resolution XPS, and the relevant spectra are shown in Figure 3 and Section 6 of the Supporting Information. Spectroscopic signatures arising from the C 1s, N 1s, and O 1s core levels associated with the grafted organic constructs along with the signal of Si 2p from the silicon substrate are unambiguously evidenced when probing the Si-NDI-15@1 and Si-NDI-2@2 surfaces. The representative high-resolution XPS spectral scans of the C 1s and N 1s regions for Si-NDI-15@1 and Si-NDI-2@2 are shown in Figure 3C and 3D and in Figure S15A and S15B, respectively. Congruent with the fact that these two hybrid interfaces comprise identical building blocks, the recorded emission features are virtually identical. The C 1s signal probed for each Si electrode can be deconvoluted into three Voigt functions with peaks centered at 288.2, 286.0, and 284.6 eV binding energies. The high-energy peak that is centered at 288.2 eV (fwhm ~ 1.7 eV) is diagnostic of oxygen-bonded (C=O) carbon atoms, whereas the emission signals centered at 286.0 eV (fwhm  $\sim 1.7$  eV) and 284.6 eV (fwhm  $\sim 1.3$  eV) are the fingerprints of nitrogen-bonded (C-N) carbon and carbonbonded (C-C) carbon atoms, respectively. While the analysis of the C 1s region may indicate the attachment of the NDI units on the Si surface, it is recognized that some unavoidable contamination from external carbon sources, notably C-O

bonds, is also at the origin of an emission signal centered at 286 eV. To circumvent this limitation, the N 1s regions recorded for the Si-NDI-15@1 and Si-NDI-2@2 surfaces shown in Figures 3D and S15B, respectively, unambiguously provide proof for the attachment of the NDI units on the Si-Az. The N 1s region for each substrate shows a broad emission signal deconvoluted into two Voigt functions with associated peaks centered at 401.9 and 400.1 eV binding energies and fwhm of 1.7 eV. These spectroscopic signatures reveal the presence of chemically distinct nitrogen atoms and confirm the attachment of the NDI cores on the Si surface.

All taken together, the XPS data confirm the formation of triazole functional moieties upon "click" reaction of the NDI module with the azide-terminated interface Si-Az. The absence of high-energy N 1s signals between 404 and 405 eV, characteristic of azide functionalities, indicates that virtually all of the terminal azide groups in Si-Az have been converted to triazole moieties. <sup>52</sup> Furthermore, a closer inspection of the high-resolution XPS spectrum of Si 2p shown in Figures S14D and S15D reveals the existence of  $\mathrm{SiO}_x$  species in negligible quantities, as evidenced by the weak emissive peak centered at 102.5 eV, suggesting that a low level of oxidation of the precursor Si–H surface has to be considered.

The potentiometric properties elucidated for the Si-NDI-15@1 and Si-NDI-2@2 interfaces differ markedly. Electrochemical measurements were performed using the Si-NDI surfaces as working electrodes, and the representative cyclic voltammograms (CVs) are shown in Figure 4. Additional CVs are shown in Figures S24 and S25. Table 1 summarizes the potentiometric properties of these interfaces. Excursion toward cathodic potentials unveils broad and ill-defined cathodic reduction waves  $E^{(p1)}$  centered at -0.150 V for Si-NDI-15@1 and −0.530 V for Si-NDI-2@2. Concomitantly, swiping back toward the anodic potentials reveals the existence of two oxidation waves  $E^{(\mathrm{p2})}$  and  $E^{(\mathrm{p3})}$  centered at  $-0.390~\mathrm{V}$  and -0.06 V for Si-NDI-15@1 and -0.850 V and -0.325 V for Si-NDI-2@2. While we acknowledge that the redox transitions appear weakly resolved even at low scan rates (25 mV s<sup>-1</sup>), these peaks are reproducible, signaling negligible surface damages under the reported experimental conditions (Figures S24 and S25). These data indicate that the Si-NDI-15@1 and Si-NDI-2@2 interfaces exhibit a partially irreversible character.

Because the electrochemical signals recorded for Si-NDI-15@1 and Si-NDI-2@2 cannot be considered reversible, we deemed it more appropriate to exploit the potentials  $E^{(i)}$ associated with the first inflection point to estimate a meaningful potential at which NDI building blocks are reduced. As shown in Figure 4, the potential associated with the first inflection point  $E^{(i1)}$  recorded for Si-NDI-15@1 is anodically shifted by more than 400 mV when compared to that elucidated for the Si-NDI-2@2 interface  $(E^{(i1)} = -0.459)$ V). Furthermore, it is interesting to note the existence of a second inflection point with an associated potential  $(E^{(i2)})$  of -0.461 V for the Si-NDI-15@1 interface and -0.802 V for the Si-NDI-2@2 interface. We postulate that  $E^{(i2)}$  diagnoses the further reduction of the NDI cores into, possibly, a dianionic species. Because the first reduction wave observed in Si-NDI-15@1 is stabilized by more than 400 mV when compared to that recorded for Si-NDI-2@2, it is fair to infer that the electronic structures and consequently the structural attributes of the NDI cores comprising the two interfaces may differ, to some extent.

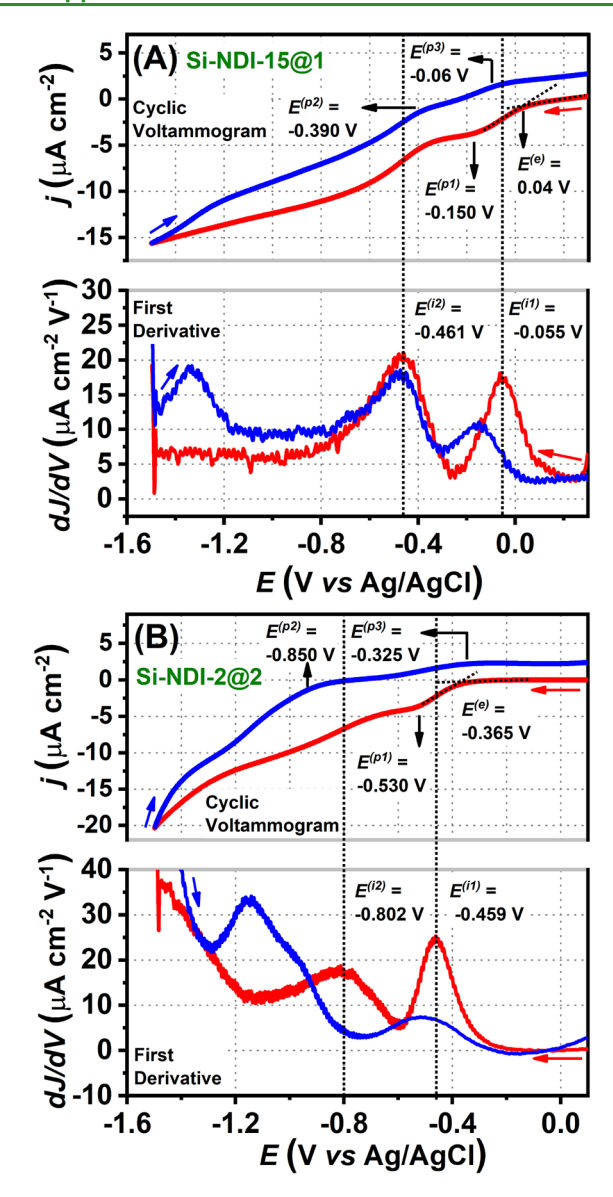


**Figure 4.** Cyclic voltammograms and their first derivative plots (scan rate = 0.025 V s<sup>-1</sup>) of **Si-NDI-15@1** (A) and **Si-NDI-2@2** (B) interfaces recorded in dry acetonitrile using 0.1 M n-Bu<sub>4</sub>NPF<sub>6</sub> as the supporting electrolyte, the **Si-NDI** surfaces as working electrodes, Ag/AgCl (3 M NaCl) as the reference electrode, and Pt as the counter electrode under Ar gas atmosphere at 25 °C. Please note that the electroactive surface area of the working electrode to convert the current ("i" in  $\mu$ A) scale to the current density ("j" in  $\mu$ A cm<sup>-2</sup>) scale was 0.5026 cm<sup>2</sup> in all the cases.

The electronic properties of NDI cores in the Si-NDI-15@1 and Si-NDI-2@2 interfaces are intimately correlated to the initial aggregation state of the redox units during the "click" reaction. In Pathway 2 leading to the Si-NDI-2@2 electrode, the NDI precursors are vastly present as a neutral, molecularly dissolved species as confirmed by ground-state electronic absorption spectroscopy. Consequently, species anchored on the Si surface originate from neutral, individualized NDI building blocks. Increasing the concentration of NDI precursors to 15 mM in Pathway 1 has a profound impact on the aggregation state of the redox-active units as mentioned earlier. As shown in Figure 1B, the spectroscopic signatures of NDI building blocks in the absence of sodium ascorbate signal a non-negligible level of NDI interactions. Further addition of

up to 1 equiv of the sacrificial electron donor used during the "click" reaction enforces the formation of  $\pi$ -anion stacks that are further anchored on the Si surface to deliver Si-NDI-15@1. The fact that Si-NDI-15@1 and Si-NDI-2@2 surfaces feature identical building block composition while electron injection is facilitated by more than 380 mV in Si-NDI-15@1 points toward the noninnocent role played by the  $\pi$ -anion stacks in regulating the final semiconducting properties of the functionalized surface. To further validate this hypothesis, additional grafting pathways were devised and are shown as Pathways 3 and 4 in Schemes 1 and 2.

Electrochemical investigation of the Si-NDI interfaces engineered via Pathways 3 and 4 (Scheme 1) confirms the noninnocent role played by the initial NDI aggregate states in dictating the potentiometric properties of Si-NDI-derived semiconducting interfaces. To isolate the effect of sodium ascorbate, Pathway 3 exploits an identical solvent mixture and initial concentration of NDI ([NDI] = 15 mM) to that used in Pathway 1 but differs in terms of the copper catalyst that was replaced by a Cu1+ source (CuI), which does not require a sacrificial electron donor. Furthermore, in Pathway 3, leading to Si-NDI-15@3, the NDI building blocks evidence a nonnegligible degree of aggregation as this pathway utilizes identical solvent composition to that of Pathway 1. Concomitantly, Pathway 4 in Scheme 1 is designed to compare the influence of the neutral NDI aggregation state of Pathway 3. Congruent with the fact that NDI building blocks demonstrate a high solubility in DMF solvent as mentioned earlier, this condition is leveraged to investigate the extent to which the anchoring of molecularly dissolved NDI units perturbs the potentiometric properties of the Si-NDI-15@4 interface and potentially contrasts that of Si-NDI-15@3. Please refer to the Supporting Information for details about the synthetic access of these interfaces (Section 2A) and their characterization using AFM (Section 5), XPS (Section 6), and electrochemistry (Section 7).

The CVs recorded for the Si-NDI-15@4 interface shown in Figure S27A feature a first reduction wave centered  $(E^{(p1)})$  at -0.510 V when swiping toward the cathodic potentials and one unresolved, weak oxidation signal  $E^{(p2)}$  centered at -0.750V when navigating back to the anodic potentials. The first derivative of the cyclic voltammogram shown in Figure S28B unveils a first reduction potential  $E^{(i)} = -0.451$  V, which is in line with the value estimated for the first reduction potentials of Si-NDI-2@2 ( $E^{(i)} = -0.459 \text{ V}$ ). Furthermore, as highlighted in Figure S27C, the concomitant increase and shift observed for these two reported potentials when increasing the scan rate may indicate that the NDI electrochemical system shows some quasi-reversible characters. The cyclic voltammogram recorded for the Si-NDI-15@3 interfaces chronicled in Figures S26A,B and S28A contrasts that acquired for Si-NDI-15@4. A weak reduction signal  $(E^{(p1)})$  is evidenced at -0.367 V, and a broad unresolved oxidation wave  $(E^{(p2)})$  is observed at -0.775 V. Similar to the Si-NDI interfaces described above, the Si-NDI-15@3 interface features two inflection points  $E^{(i1)}$  and  $E^{(i2)}$ centered at -0.273 V and -0.785 V, respectively. It is interesting to note that the  $E^{(ii)}$  recorded for  $\hat{Si}$ -NDI-15@3 is stabilized by more than 170 mV when compared to that calculated for Si-NDI-15@4 but destabilized by more than 200 mV when compared to that elucidated for the Si-NDI-15@1

Comparing the first inflection point potentials  $E^{(i)}$  measured for the Si-NDI-15@3 and Si-NDI-15@1 interfaces further

Table 1. Potentiometric Properties of Diverse Si-NDI Interfaces Accessed via Different Azide—Alkyne "Click" Reaction Conditions

pathways/Si-NDI interfaces <sup>a</sup>	potentiometric properties <sup>b</sup>					
	$E^{(p1)}$ (V)	$E^{(p2)}$ (V)	$E^{(p3)}$ (V)	E <sup>(e)</sup> (V)	E <sup>(i1)</sup> (V)	$E^{(i2)}(V)$
1/Si-NDI-15@1	-0.150	-0.390	-0.060	0.040	-0.055	-0.461
2/Si-NDI-2@2	-0.530	-0.850	-0.325	-0.365	-0.459	-0.802
3/Si-NDI-15@3	-0.367	-0.775	N/A	-0.225	-0.273	-0.785
4/Si-NDI-15@4	-0.510	-0.750	N/A	-0.331	-0.451	-0.730
5/Si(1:50)-NDI-15@5	-0.540	-0.865	N/A	-0.323	-0.398	-0.730

"All the "click" reactions were carried out under Ar gas atmosphere in degassed solvent/media at rt for 24 h. During all the "click" reactions, the amount of the Cu salt (i.e., CuSO<sub>4</sub> or CuI) employed was 10 mol % with respect to NDI, and the amount of the base (i.e., Na-ascorbate or Hünig's base) employed was 10 mol equiv with respect to the Cu salt, hence 1 mol equiv with respect to NDI, cf. SI for details. <sup>b</sup>All the cyclic voltammetric experiments were carried out under Ar gas atmosphere at 25 °C in dry acetonitrile using 0.1 M n-Bu<sub>4</sub>NPF<sub>6</sub> as the supporting electrolyte, the Si-NDI surfaces as working electrodes, Ag/AgCl (3 M NaCl) as the reference electrode, and Pt as the counter electrode. The electroactive surface area for all the measurements was 0.5026 cm<sup>2</sup>. Each measurement has been reproduced 3 times at different spots on the surface. Please note that  $E^{(p)}$ ,  $E^{(e)}$ , and  $E^{(i)}$  refer to peak potential, edge potential, and potential at the inflection point of the cathodic wave, respectively. N/A refers to the absence of any discernible peak. The potential values are reported versus Ag/AgCl (3 M NaCl) as the reference. Please refer to Section 7 in the Supporting Information for details.

supports the noninnocent role played by the NDI  $\pi$ -anion stacks. While the initial NDI precursors exist as partially aggregated in the experimental conditions employed in Pathway 3, the lack of sacrificial electron donor in the "click" reaction conditions prevents the formation of n-doped aggregates. In this regard, we postulate that the NDI species anchored on the Si surface in Pathway 3 does not share the same initial structure–function relationships as the NDI  $\pi$ anion stacks exclusively generated in Pathway 1. Because the electronic properties of the grafted NDI domains are intimately correlated to the magnitude of the interaction between the redox-active units and the conformation of the building blocks, the difference of semiconducting properties evidenced by Si-**NDI-15@3**  $(E^{(i1)} = -0.273 \text{ V})$  and **Si-NDI-15@1**  $(E^{(i1)} =$ -0.055 V) interfaces originates from the structure-function relationships of the parent NDI precursors.

While the semiconducting Si-NDI-15@4 interface has been constructed using a high concentration of NDI units ([NDI] = 15 mM), its first reduction potential  $(E^{(i1)} = -0.451 \text{ V})$ resembles that recorded for Si-NDI-2@2 ( $E^{(i1)} = -0.459 \text{ V}$ ). It is interesting to correlate the electronic functions of these two interfaces with the aggregated states of the precursor NDI building blocks. In Pathway 4 that exploits a 15 mM concentration of NDI units in DMF solvent, the building blocks exist as molecularly dissolved. Similarly, the NDI cores are individualized under the conditions used in Pathway 2  $(MeOH/H_2O, [NDI] = 2 \text{ mM})$ . All taken together, these data underscore the importance of the initial aggregated state of the NDI units and indicate that the first reduction potentials measured for the Si-NDI-15@4 and Si-NDI-2@2 interfaces originate from NDI domains constructed from individualized redox-active units during the "click" reaction.

Additional proof that the initial aggregated state of NDI building blocks offers a means to regulate the semiconducting properties of functionalized Si interfaces stems from comparing the first reduction potentials recorded for Si-NDI-15@3 and Si-NDI-15@4. Please note that the Si-NDI-15@3 interface is constructed by exploiting NDI precursors (Pathway 3, Scheme 1) with a non-negligible degree of aggregation as confirmed by electronic absorption spectroscopy. Chronicled in Table 1, a more positive potential is required to inject electrons in Si-NDI-15@3 ( $E^{(i1)} = -0.273$  V) when compared to Si-NDI-15@4 ( $E^{(i1)} = -0.451$  V). It is interesting to corroborate this

finding with the potentiometric properties recorded for the solution-based NDI precursors shown in Figure 2. The aggregation of NDI units at high concentration enforces the formation of a solvated species that features a more positive first reduction potential ( $\Delta E^{(i1)} = 160 \text{ mV}$ ) with respect to that of the molecularly dissolved species. This observation signals the formation of electronic states in solvated NDI aggregates that facilitate electron transfer. Similarly, we hypothesize that NDI domains in Si-NDI-15@3 may feature a non-negligible degree of NDI-NDI interaction dialed-in by the solvated precursor building blocks.

The engineering of a Si precursor surface characterized by a low density of anchoring groups confirms that the potentiometric properties recorded for Si-NDI-15@1 stem from NDI units, evidencing a non-negligible degree of aggregation. It is expected that a silicon surface equipped with a low density of reactive azide groups may not be capable of fully trapping the NDI aggregate formed in solution and would rather only capture one or some of the repeating units forming the aggregates. The mixed-acetylene functionalized interface Si-(1:50)-Oct shown in Figure S1 was engineered by covalent modification of Si(111)-H via a thermally activated grafting mechanism with a 1:50 molar ratio mixture of 1,7-octadiyne and 1-octyne. Further functionalization of the residual terminal alkyne with diazidoethane by means of a "click" reaction produces the diluted surface precursor Si(1:50)-Az. Please refer to Section 2 of the Supporting Information for more details. Assessing the surface coverage using ferrocene probes reveals an azide surface coverage of  $8.44 \times 10^{-12}$  mol cm<sup>-2</sup>. This surface coverage correlates to a density of one azide function per 20 nm<sup>2</sup>. Notably, a similar approach has been reported for a mixed diyne-functionalized surface by Ciampi and co-workers. <sup>41</sup> The Si(1:50)-Az surface that features a low density of anchoring sites is subjected to the functionalization Pathway 5 to deliver the Si(1:50)-NDI-15@5 interface shown in Figure S1. The characterization data related to AFM (Figure S13) and XPS (Figure S18) of this interface are chronicled in the Supporting Information. Please note that Pathway 5 exploits identical experimental conditions to those of Pathway 1 but differs in the nature of the silicon precursor that features a lower density of azide anchoring groups.

The electrochemical characterization of Si(1:50)-NDI-15@ 5 using cyclic voltammetry ( $\nu = 0.025 \text{ V/s}$ ) in acetonitrile is

shown in Figure 5 and reveals that the potentiometric properties ( $E^{(i1)} = -0.398$  V) differ remarkably from those

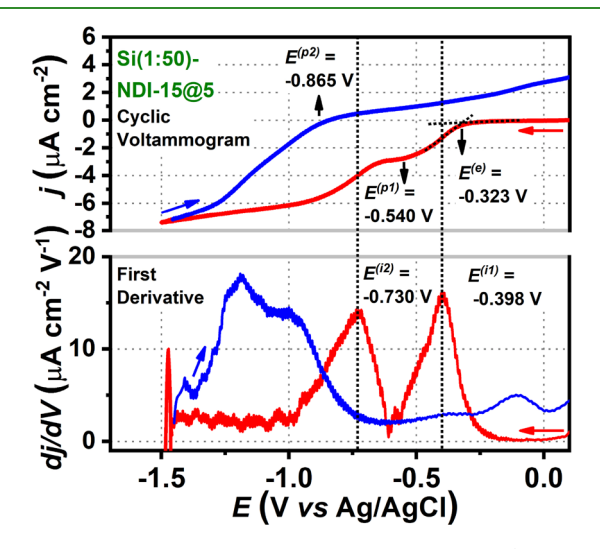


**Figure 5.** Cyclic voltammogram and its first derivative (scan rate =  $0.025 \text{ V s}^{-1}$ ) of the surface-diluted **Si(1:50)-NDI-15@5** recorded in dry acetonitrile using  $0.1 \text{ M } n\text{-Bu}_4\text{NPF}_6$  as the supporting electrolyte, the **Si-NDI** surface as the working electrode, Ag/AgCl (3 M NaCl) as the reference electrode, and Pt as the counter electrode under Ar gas atmosphere at 25 °C.

of Si-NDI-15@1 ( $E^{(i1)} = -0.055$  V), but surprisingly they are comparable to those recorded for Si-NDI-15@4 ( $E^{(i1)} = -0.451$  V) and Si-NDI-2@2 ( $E^{(i1)} = -0.459$  V). Because lateral NDI-NDI interaction in Si(1:50)-NDI-15@5 is likely to be suppressed due to the low density of anchoring points, we postulate that the potentiometric properties recorded for Si(1:50)-NDI-15@5 are characteristic of the individualized redox-active cores on silicon electrodes. It is important to emphasize that both Si(1:50)-NDI-15@5 and Si-NDI-15@1 leverage the NDI  $\pi$ -anion stacks as precursors but that these two interfaces demonstrate substantially different potentiometric properties.

While a matter of speculation at this time, we believe that the surface-diluted Si(1:50)-Az precursor does not provide a density of reactive groups high enough to fully anchor the  $\pi$ anion stack aggregates formed in solution. During the "click" reaction, only one or some of the NDI units composing the aggregates are anchored on the diluted surface. It is fair to assume that the NDI units not covalently grafted on the Si surface are washed away during the postsynthesis workup treatment. In sharp contrast, the electrochemical data presented for Si-NDI-15@1 are representative of the aggregated NDI units anchored on the surface. Because the precursor Si-Az surface presents a high density of reactive azide functions, it enables the trapping of the NDI aggregates, initially formed in Pathway 1, in its full integrity. The fact that electron injection is facilitated in Si-NDI-15@1 when compared to Si(1:50)-NDI-15@5 may originate from the existence of delocalized states enforced by interactions of NDI cores on the Si surfaces.

# CONCLUSIONS

A set of redox-active hybrid Si interfaces Si-NDIs have been developed through the covalent functionalization of Si(111)-H with a naphthalene diimide-based n-type molecular system.

The multistep synthetic grafting strategy to access the Si-NDI interfaces involves a thermally activated grafting of an aliphatic divne on Si(111)-H, followed by postsynthetic modifications using "click" reactions. Subtle variations of the NDI-aggregated states during the "click" reaction are shown to modulate the potentiometric properties characterizing the hybrid interfaces. In this regard, grafting NDI  $\pi$ -anion stacks on the Si surfaces delivers the semiconducting Si surface Si-NDI-15@1 for which electron injection occurs at more positive potentials ( $E^{(i1)}$  = -0.055 V) with respect to the Si surfaces Si-NDI-2@2 ( $E^{(i1)}$  = -0.459 V) and Si-NDI-15@4 ( $E^{(i1)} = -0.451 \text{ V}$ ) built from individualized NDI units. Furthermore, we show that the anchorage of a neutral NDI aggregate on a Si interface offers the Si-NDI-15@3 interface which does not facilitate electron injection ( $E^{(i1)} = -0.273 \text{ V}$ ) with the same magnitude of that observed for the Si-NDI-15@1 interface.

To reveal the noninnocent roles played by interchromophore interaction and conformation at the interface in regulating the overall potentiometric properties, a "surface dilution" experiment was carried out to access the Si(1:50)-NDI-15@5 interface by sequential "click" reactions on a mixed-acetylene functionalized Si surface. This interface is characterized by a low density of NDI units that averages ~1 core per 20 nm<sup>2</sup>. While constructed under identical synthetic conditions as the Si-NDI-15@1 interface, the functionalized Si(1:50)-NDI-15@5 electrode exhibits potentiometric properties  $(E^{(i1)} = -0.398 \text{ V})$  matching those observed in the case of Si-NDI-15@4  $(E^{(i1)} = -0.451 \text{ V})$  and Si-NDI-2@2  $(E^{(i1)} =$ -0.459 V). This observation suggests the existence of an electronic state reminiscent to that of individualized NDI chromophores at the Si(1:50)-NDI-15@5 interface. This assumption is further supported by the fact that the interactions between the chromophores are negligibly small due to the smaller number of NDI chromophores in close proximity due to the "surface dilution" effect.

To summarize, the results reported herein reveal that the potentiometric properties of hybrid Si-NDI interfaces can be modulated by the initial aggregation states of the NDI redox probe covalently anchored on Si surfaces. Because examples that delineate the functionalization of Si electrodes with electron-deficient molecular components are scarce, these findings may open new avenues to construct n-type semiconducting hybrid materials. Furthermore, considering the ever-growing importance of functional hybrid interfaces, this study delineates new tools for the development of functionalized microelectronics and can pave the way to engineer novel classes of electroactive materials.

#### ASSOCIATED CONTENT

## Supporting Information

The Supporting Information is available free of charge at https://pubs.acs.org/doi/10.1021/acsami.0c18222.

Synthetic details, sample preparation, ground-state electronic absorption spectra, spectroelectrochemistry, AFM images, XPS spectra and electrochemistry via cyclic voltammetry (PDF)

# AUTHOR INFORMATION

# **Corresponding Author**

Jean-Hubert Olivier – Department of Chemistry, University of Miami, Coral Gables, Florida 33146, United States;

o orcid.org/0000-0003-0978-4107; Phone: +1 305 284 3279; Email: jh.olivier@miami.edu

#### **Authors**

Arindam Mukhopadhyay — Department of Chemistry, University of Miami, Coral Gables, Florida 33146, United States; © orcid.org/0000-0002-0620-4157

Victor Paulino – Department of Chemistry, University of Miami, Coral Gables, Florida 33146, United States

Kaixuan Liu – Department of Chemistry, University of Miami, Coral Gables, Florida 33146, United States

Carrie L. Donley — Chapel Hill Analytical and Nanofabrication Laboratory, Department of Applied Physical Sciences, University of North Carolina, Chapel Hill, North Carolina 27599, United States; orcid.org/0000-0003-0906-306X

Brianna Bernard – Department of Chemistry, University of Miami, Coral Gables, Florida 33146, United States

Alfred Shomar – Department of Chemistry, University of Miami, Coral Gables, Florida 33146, United States

Chuan Liu – Department of Chemistry, University of Miami, Coral Gables, Florida 33146, United States

Complete contact information is available at: https://pubs.acs.org/10.1021/acsami.0c18222

#### **Notes**

The authors declare no competing financial interest.

# ACKNOWLEDGMENTS

Our Si surface functionalization work is supported by the Arnold and Mabel Beckman Foundation under award BYI 2018, and our work on redox-assisted assembly of  $\pi$ -conjugated chromophores is supported by the National Science Foundation under the CAREER award CHE-1941410. XPS analysis was performed at the Chapel Hill Analytical and Nanofabrication Laboratory, CHANL, a member of the North Carolina Research Triangle Nanotechnology Network, RTNN, which is supported by the National Science Foundation, Grant CCS-1542015, as part of the National Nanotechnology Coordinated Infrastructure, NNCI. We thank Prof. Roger Leblanc for giving us access to his atomic force microscope.

### REFERENCES

- (1) Bloom, B. P.; Liu, R.; Zhang, P.; Ghosh, S.; Naaman, R.; Beratan, D. N.; Waldeck, D. H. Directing Charge Transfer in Quantum Dot Assemblies. *Acc. Chem. Res.* **2018**, *51* (10), 2565–2573.
- (2) Younts, R.; Duan, H.-S.; Gautam, B.; Saparov, B.; Liu, J.; Mongin, C.; Castellano, F. N.; Mitzi, D. B.; Gundogdu, K. Efficient Generation of Long-Lived Triplet Excitons in 2D Hybrid Perovskite. *Adv. Mater.* **2017**, 29 (9), 1604278.
- (3) McCusker, C.; Castellano, F. Materials Integrating Photochemical Upconversion; 2017; pp 175–199.
- (4) Facchetti, A.  $\pi$ -Conjugated Polymers for Organic Electronics and Photovoltaic Cell Applications. *Chem. Mater.* **2011**, 23 (3), 733–758.
- (5) Samorí, P.; Feng, X.; Bonifazi, D.  $\pi$ -Conjugated Molecules: From Structure to Function. *ChemPlusChem* **2019**, 84 (9), 1177–1178.
- (6) Faramarzi, V.; Niess, F.; Moulin, E.; Maaloum, M.; Dayen, J.-F.; Beaufrand, J.-B.; Zanettini, S.; Doudin, B.; Giuseppone, N. Light-triggered Self-Construction of Supramolecular Organic Nanowires as Metallic Interconnects. *Nat. Chem.* **2012**, *4*, 485.
- (7) Armao, J. J.; Maaloum, M.; Ellis, T.; Fuks, G.; Rawiso, M.; Moulin, E.; Giuseppone, N. Healable Supramolecular Polymers as Organic Metals. J. Am. Chem. Soc. 2014, 136 (32), 11382–11388.

- (8) Bullard, G.; Tassinari, F.; Ko, C.-H.; Mondal, A. K.; Wang, R.; Mishra, S.; Naaman, R.; Therien, M. J. Low-Resistance Molecular Wires Propagate Spin-Polarized Currents. *J. Am. Chem. Soc.* **2019**, *141* (37), 14707–14711.
- (9) Göhler, B.; Hamelbeck, V.; Markus, T. Z.; Kettner, M.; Hanne, G. F.; Vager, Z.; Naaman, R.; Zacharias, H. Spin Selectivity in Electron Transmission Through Self-Assembled Monolayers of Double-Stranded DNA. *Science* **2011**, *331*, 894–897.
- (10) Fontanesi, C.; Capua, E.; Paltiel, Y.; Waldeck, D. H.; Naaman, R. Spin-Dependent Processes Measured without a Permanent Magnet. *Adv. Mater.* **2018**, *30*, 1707390.
- (11) Kulkarni, C.; Mondal, A. K.; Das, T. K.; Grinbom, G.; Tassinari, F.; Mabesoone, M. F. J.; Meijer, E. W.; Naaman, R. Highly Efficient and Tunable Filtering of Electrons' Spin by Supramolecular Chirality of Nanofiber-Based Materials. *Adv. Mater.* **2020**, 32 (7), 1904965.
- (12) Zhou, H.; Yang, L.; You, W. Rational Design of High Performance Conjugated Polymers for Organic Solar Cells. *Macromolecules* **2012**, *45* (2), 607–632.
- (13) Price, S. C.; Stuart, A. C.; Yang, L.; Zhou, H.; You, W. Fluorine Substituted Conjugated Polymer of Medium Band Gap Yields 7% Efficiency in Polymer-Fullerene Solar Cells. *J. Am. Chem. Soc.* **2011**, 133 (12), 4625–4631.
- (14) Rawson, J.; Stuart, A. C.; You, W.; Therien, M. J. Tailoring Porphyrin-Based Electron Accepting Materials for Organic Photovoltaics. *J. Am. Chem. Soc.* **2014**, *136* (50), 17561–17569.
- (15) Wasielewski, M. R. Self-Assembly Strategies for Integrating Light Harvesting and Charge Separation in Artificial Photosynthetic Systems. *Acc. Chem. Res.* **2009**, *42* (12), 1910–1921.
- (16) Song, R.; Wang, Z.; Zhou, X.; Huang, L.; Chi, L. Gas-Sensing Performance and Operation Mechanism of Organic  $\pi$ -Conjugated Materials. *ChemPlusChem* **2019**, 84 (9), 1222–1234.
- (17) Schroeder, V.; Savagatrup, S.; He, M.; Lin, S.; Swager, T. M. Carbon Nanotube Chemical Sensors. *Chem. Rev.* **2019**, *119* (1), 599–663.
- (18) Buriak, J. M. Organometallic Chemistry on Silicon and Germanium Surfaces. *Chem. Rev.* **2002**, *102* (5), 1271–1308.
- (19) McCreery, R. L. Molecular Electronic Junctions. *Chem. Mater.* **2004**, *16* (23), 4477–4496.
- (20) Onclin, S.; Ravoo, B. J.; Reinhoudt, D. N. Engineering Silicon Oxide Surfaces Using Self-Assembled Monolayers. *Angew. Chem., Int. Ed.* **2005**, 44 (39), 6282–6304.
- (21) Love, J. C.; Estroff, L. A.; Kriebel, J. K.; Nuzzo, R. G.; Whitesides, G. M. Self-Assembled Monolayers of Thiolates on Metals as a Form of Nanotechnology. *Chem. Rev.* **2005**, *105* (4), 1103–1170.
- (22) Ciampi, S.; Harper, J. B.; Gooding, J. J. Wet Chemical Routes to the Assembly of Organic Monolayers on Silicon Surfaces via theFormation of Si-C bonds: Surface Preparation, Passivation and functionalization. *Chem. Soc. Rev.* **2010**, *39* (6), 2158–2183.
- (23) Gooding, J. J.; Ciampi, S. The Molecular Level Modification of Surfaces: from Self-Assembled Monolayers to Complex Molecular Assemblies. *Chem. Soc. Rev.* **2011**, *40* (5), 2704–2718.
- (24) Fabre, B. Functionalization of Oxide-Free Silicon Surfaces with Redox-Active Assemblies. *Chem. Rev.* **2016**, *116* (8), 4808–4849.
- (25) Beiler, A. M.; Khusnutdinova, D.; Wadsworth, B. L.; Moore, G. F. Cobalt Porphyrin-Polypyridyl Surface Coatings for Photoelectrosynthetic Hydrogen Production. *Inorg. Chem.* **2017**, *56* (20), 12178–12185.
- (26) Wadsworth, B. L.; Khusnutdinova, D.; Urbine, J. M.; Reyes, A. S.; Moore, G. F. Expanding the Redox Range of Surface-Immobilized Metallocomplexes Using Molecular Interfaces. *ACS Appl. Mater. Interfaces* **2020**, *12* (3), 3903–3911.
- (27) Linford, M. R.; Fenter, P.; Eisenberger, P. M.; Chidsey, C. E. Alkyl Monolayers on Silicon Prepared from 1-Alkenes and Hydrogen-Terminated Silicon. *J. Am. Chem. Soc.* **1995**, *117* (11), 3145–3155.
- (28) Buriak, J. M. Illuminating Slicon Surface Hydrosilylation: an Unexpected Plurality of Mechanisms. *Chem. Mater.* **2014**, *26* (1), 763–772.

- (29) Ciampi, S.; James, M.; Darwish, N.; Luais, E.; Guan, B.; Harper, J. B.; Gooding, J. J. Oxidative Acetylenic Coupling Reactions as a Surface Chemistry Tool. *Phys. Chem. Chem. Phys.* **2011**, *13* (34), 15624–15632.
- (30) Ciampi, S.; James, M.; Michaels, P.; Gooding, J. J. Tandem "click" Reactions at Acetylene-Terminated Si (100) Monolayers. *Langmuir* **2011**, 27 (11), 6940–6949.
- (31) Ciampi, S.; James, M.; Le Saux, G.; Gaus, K.; Justin Gooding, J. Electrochemical "Switching" of Si (100) Modular Assemblies. *J. Am. Chem. Soc.* **2012**, *134* (2), 844–847.
- (32) Lattimer, J. R.; Brunschwig, B. S.; Lewis, N. S.; Gray, H. B. Redox Properties of Mixed Methyl/Vinylferrocenyl Monolayers on Si (111) Surfaces. *J. Phys. Chem. C* **2013**, *117* (51), 27012–27022.
- (33) O'Leary, L. E.; Rose, M. J.; Ding, T. X.; Johansson, E.; Brunschwig, B. S.; Lewis, N. S. Heck Coupling of Olefins to Mixed Methyl/Thienyl Monolayers on Si (111) Surfaces. *J. Am. Chem. Soc.* **2013**, *135* (27), 10081–10090.
- (34) Fabre, B.; Pujari, S. P.; Scheres, L.; Zuilhof, H. Micropatterned Ferrocenyl Monolayers Covalently Bound to Hydrogen-Terminated Silicon Surfaces: Effects of Pattern Size on the Cyclic Voltammetry and Capacitance Characteristics. *Langmuir* **2014**, *30* (24), 7235–7243.
- (35) Yang, Y.; Ciampi, S.; Choudhury, M. H.; Gooding, J. J. Light Activated Electrochemistry: Light Intensity and pH Dependence on Electrochemical Performance of Anthraquinone Derivatized Silicon. *J. Phys. Chem. C* **2016**, *120* (5), 2874–2882.
- (36) Fabre, B.; Hauquier, F. Boronic Acid-Functionalized Oxide-Free Silicon Surfaces for the Electrochemical Sensing of Dopamine. *Langmuir* **2017**, 33 (35), 8693–8699.
- (37) Decker, F.; Cattaruzza, F.; Coluzza, C.; Flamini, A.; Marrani, A. G.; Zanoni, R.; Dalchiele, E. A. Electrochemical Reversibility of Vinylferrocene Monolayers Covalently Attached on H-Terminated p-Si (100). *J. Phys. Chem. B* **2006**, *110* (14), 7374–7379.
- (38) Tajimi, N.; Sano, H.; Murase, K.; Lee, K.-H.; Sugimura, H. Thermal Immobilization of Ferrocene Derivatives on (111) Surface of n-type Silicon: Parallel Between Vinylferrocene and Ferrocenecarbox-aldehyde. *Langmuir* **2007**, 23 (6), 3193–3198.
- (39) Hauquier, F.; Ghilane, J.; Fabre, B.; Hapiot, P. Conducting Ferrocene Monolayers on Nonconducting Surfaces. *J. Am. Chem. Soc.* **2008**, *130* (9), 2748–2749.
- (40) Gauthier, N.; Argouarch, G.; Paul, F.; Humphrey, M. G.; Toupet, L.; Ababou-Girard, S.; Sabbah, H.; Hapiot, P.; Fabre, B. Silicon Surface-Bound Redox-Active Conjugated Wires Derived From Mono-and Dinuclear Iron (II) and Ruthenium (II) Oligo (phenyleneethynylene) Complexes. *Adv. Mater.* **2008**, 20 (10), 1952–1956.
- (41) Ciampi, S.; Eggers, P. K.; Le Saux, G.; James, M.; Harper, J. B.; Gooding, J. J. Silicon (100) Electrodes Resistant to Oxidation in Aqueous Solutions: an Unexpected Benefit of Surface Acetylene Moieties. *Langmuir* **2009**, 25 (4), 2530–2539.
- (42) Ciampi, S.; Luais, E.; James, M.; Choudhury, M. H.; Darwish, N. A.; Gooding, J. J. The Rapid Formation of Functional Monolayers on Silicon Under Mild Conditions. *Phys. Chem. Chem. Phys.* **2014**, *16* (17), 8003–8011.
- (43) Gosztola, D.; Niemczyk, M. P.; Svec, W.; Lukas, A. S.; Wasielewski, M. R. Excited Doublet States of Electrochemically Generated Aromatic Imide and Diimide radical anions. *J. Phys. Chem. A* **2000**, *104* (28), 6545–6551.
- (44) Sakai, N.; Mareda, J.; Vauthey, E.; Matile, S. Core-substituted Naphthalenediimides. *Chem. Commun.* **2010**, *46* (24), 4225–4237.
- (45) Kobr, L. s.; Gardner, D. M.; Smeigh, A. L.; Dyar, S. M.; Karlen, S. D.; Carmieli, R.; Wasielewski, M. R. Fast Photodriven Electron Spin Coherence TRansfer: a Quantum Gate based on a Spin Exchange J-jump. *J. Am. Chem. Soc.* **2012**, *134* (30), 12430–12433.
- (46) Roznyatovskiy, V. V.; Gardner, D. M.; Eaton, S. W.; Wasielewski, M. R. Radical Anions of Trifluoromethylated perylene and Naphthalene Imide and Diimide Electron Acceptors. *Org. Lett.* **2014**, *16* (3), 696–699.

- (47) Al Kobaisi, M.; Bhosale, S. V.; Latham, K.; Raynor, A. M.; Bhosale, S. V. Functional Naphthalene Diimides: Synthesis, Properties, and Applications. *Chem. Rev.* **2016**, *116* (19), 11685–11796.
- (48) Nowak-Król, A.; Shoyama, K.; Stolte, M.; Würthner, F. Naphthalene and Perylene Diimides-better Alternatives to Fullerenes for Organic Electronics? *Chem. Commun.* **2018**, *54* (98), 13763–13772.
- (49) Bullock, J. E.; Vagnini, M. T.; Ramanan, C.; Co, D. T.; Wilson, T. M.; Dicke, J. W.; Marks, T. J.; Wasielewski, M. R. Photophysics and Redox Properties of Rylene Imide and Diimide Dyes Alkylated Ortho to the Imide Groups. *J. Phys. Chem. B* **2010**, *114* (5), 1794–1802.
- (50) Jiang, W.; Li, Y.; Wang, Z. Tailor-Made Rylene Arrays for High Performance n-channel Semiconductors. *Acc. Chem. Res.* **2014**, 47 (10), 3135–3147.
- (51) Chen, L.; Li, C.; Müllen, K. Beyond Perylene Diimides: Synthesis, Assembly and Function of Higher Rylene Chromophores. *J. Mater. Chem. C* **2014**, 2 (11), 1938–1956.
- (52) Mukhopadhyay, A.; Bernard, B.; Liu, K.; Paulino, V.; Liu, C.; Donley, C.; Olivier, J.-H. Molecular Strategies to Modulate the Electrochemical Properties of P-Type Si (111) Surfaces Covalently Functionalized with Ferrocene and Naphthalene Diimide. *J. Phys. Chem. B* **2019**, *123* (51), 11026–11041.
- (53) Ashcraft, A.; Liu, K.; Mukhopadhyay, A.; Paulino, V.; Liu, C.; Bernard, B.; Husainy, D.; Phan, T.; Olivier, J.-H. A Molecular Strategy to Lock-in the Conformation of a Perylene Bisimide-Derived Supramolecular Polymer. *Angew. Chem., Int. Ed.* **2020**, *59* (19), 7487–7493.
- (54) Liu, C.; Liu, K.; Klutke, J.; Ashcraft, A.; Steefel, S.; Olivier, J.-H. Deciphering the Potentiometric Properties of (Porphinato)zinc(ii)-Derived Supramolecular Polymers and Related Superstructures. *J. Mater. Chem. C* **2018**, *6* (44), 11980–11991.
- (55) Liu, C.; Liu, K.; Mukhopadhyay, A.; Paulino, V.; Bernard, B.; Olivier, J.-H. Butadiyne-Bridged (Porphinato)Zinc(II) Chromophores Assemble into Free-Standing Nanosheets. *Organometallics* **2020**, 39 (16), 2984–2990.
- (56) De Greef, T. F. A.; Smulders, M. M. J.; Wolffs, M.; Schenning, A. P. H. J.; Sijbesma, R. P.; Meijer, E. W. Supramolecular Polymerization. *Chem. Rev.* **2009**, *109* (11), 5687–5754.
- (57) Grimme, S. Do Special Noncovalent  $\pi$ - $\pi$  Stacking Interactions Really Exist? *Angew. Chem., Int. Ed.* **2008**, 47 (18), 3430–3434.
- (58) Cozzi, F.; Ponzini, F.; Annunziata, R.; Cinquini, M.; Siegel, J. S. Polar Interactions between Stacked  $\pi$  Systems in Fluorinated 1,8-Diarylnaphthalenes: Importance of Quadrupole Moments in Molecular Recognition. *Angew. Chem., Int. Ed. Engl.* **1995**, 34 (9), 1019–1020.
- (59) Salonen, L. M.; Ellermann, M.; Diederich, F. Aromatic Rings in Chemical and Biological Recognition: Energetics and Structures. *Angew. Chem., Int. Ed.* **2011**, *50* (21), 4808–4842.
- (60) Shao, H.; Nguyen, T.; Romano, N. C.; Modarelli, D. A.; Parquette, J. R. Self-Assembly of 1-D n-Type Nanostructures Based on Naphthalene Diimide-Appended Dipeptides. *J. Am. Chem. Soc.* **2009**, *131* (45), 16374–16376.
- (61) Molla, M. R.; Ghosh, S. Structural Variations on Self-Assembly and Macroscopic Properties of 1,4,5,8-Naphthalene-diimide Chromophores. *Chem. Mater.* **2011**, 23 (1), 95–105.
- (62) Molla, M. R.; Ghosh, S. Aqueous Self-Assembly of Chromophore-Conjugated Amphiphiles. *Phys. Chem. Chem. Phys.* **2014**, 16 (48), 26672–26683.
- (63) Miller, L. L.; Mann, K. R.  $\pi$ -Dimers and  $\pi$ -Stacks in Solution and in Conducting Polymers. Acc. Chem. Res. 1996, 29 (9), 417–423.
- (64) Ashkenasy, N.; Horne, W. S.; Ghadiri, M. R. Design of Self-Assembling Peptide Nanotubes With Delocalized Electronic States. *Small* **2006**, 2 (1), 99–102.
- (65) Avestro, A. J.; Gardner, D. M.; Vermeulen, N. A.; Wilson, E. A.; Schneebeli, S. T.; Whalley, A. C.; Belowich, M. E.; Carmieli, R.; Wasielewski, M. R.; Stoddart, J. F. Gated Electron Sharing Within Dynamic Naphthalene Diimide-Based Oligorotaxanes. *Angew. Chem., Int. Ed.* **2014**, 53 (17), 4442–4449.

- (66) Wu, Y.; Frasconi, M.; Gardner, D. M.; McGonigal, P. R.; Schneebeli, S. T.; Wasielewski, M. R.; Stoddart, J. F. Electron Delocalization in a Rigid Cofacial Naphthalene-1, 8:4, 5-bis (dicarboximide) Dimer. *Angew. Chem., Int. Ed.* **2014**, 53 (36), 9476–9481.
- (67) Espinoza, E. M.; Clark, J. A.; Soliman, J.; Derr, J. B.; Morales, M.; Vullev, V. I. Practical Aspects of Cyclic Voltammetry: How to Estimate Reduction Potentials when Irreversibility Prevails. *J. Electrochem. Soc.* **2019**, *166* (5), H3175.
- (68) Tu, Y.-J.; Njus, D.; Schlegel, H. B. A Theoretical Study of Ascorbic Acid Oxidation and HOO/O2- Radical Scavenging. *Org. Biomol. Chem.* **2017**, *15* (20), 4417–4431.
- (69) Liu, K.; Levy, A.; Liu, C.; Olivier, J.-H. Tuning Structure-Function Properties of π-Conjugated Superstructures by Redox-Assisted Self-Assembly. *Chem. Mater.* **2018**, 30 (6), 2143–2150.
- (70) Liu, K.; Mukhopadhyay, A.; Ashcraft, A.; Liu, C.; Levy, A.; Blackwelder, P.; Olivier, J.-H. Reconfiguration of  $\pi$ -Conjugated Superstructures Enabled by Redox-Assisted Assembly. *Chem. Commun.* **2019**, 55 (39), 5603–5606.